Experiments in Fluids 16 (1994) 393–400 © Springer Verlag 1994

Neutrally buoyant bubbles used as flow tracers in air

Michael F. Kerho, Michael B. Bragg

Abstract Research has been performed to determine the accuracy of neutrally buoyant and near-neutrally-buoyant bubbles used as flow tracers in an incompressible potential flowfield. Experimental and computational results are presented to evaluate the quantitative accuracy of neutrally buoyant bubbles using a commercially available helium bubble generation system. A two-dimensional experiment was conducted to determine actual bubble trajectories in the stagnation region of a NACA 0012 airfoil at 0° angle of attack. A computational scheme evaluating the equation of motion for a single bubble was also used to determine the factors which affect a bubble's trajectory. The theoretical and computational analysis have shown that neutrally buoyant bubbles will trace complex flow patterns faithfully in the flowfield of interest. Experimental analysis revealed that the use of bubbles generated by the commercially available system to trace flow patterns should be limited to qualitative measurements unless care is taken to ensure neutral buoyancy.

Nomenclature

Symbol	Description
a_c	centripetal acceleration
c	model chord
C_D	bubble drag coefficient
D	bubble diameter
g	acceleration due to gravity
g_v	acceleration due to gravity vector
h	trajectory deviation normalization parameter
K	nondimensional inertia parameter, $\sigma D^2 U_\infty / 18 c\mu$
m_f	mass of fluid
m_p	mass of bubble
p	static pressure
r	radial distance, bubble radius
R	gas constant
Re	free-stream Reynolds number, $\rho c U_\infty / \mu$
Re_p	bubble slip Reynolds number, $(\rho D U_\infty / \mu) \lvert v_p - v_f \rvert$
S	cross-sectional area of sphere
T	temperature
t	time
u	streamwise velocity component
U_∞	free-stream velocity
v_f	fluid velocity vector
v_p	bubble velocity vector
x_p	bubble position vector
y_b	bubble trajectory y/c
y_S	streamline y/c
α	model angle of attack
γ	bubble solution surface tension
Γ	potential vortex strength
ρ_{bfs}	bubble solution density
ρ	fluid density
σ	bubble density
τ	bubble wall thickness
μ	fluid viscosity

Received: 1 March 1993 / Accepted: 28 December 1993

Michael F. Kerho, Michael B. Bragg
The University of Illinois at Urbana-Champaign, Department of Aeronautical and Astronautical Engineering, 306 Talbot Laboratory, 104 South Wright Street, Urbana, IL 61801-2935, USA

1 Introduction

The understanding of complex fluid-dynamic processes has always been aided by insight manifested through physical visualization of the flowfield. The most common method of flow visualization in air is smoke. For a complex unsteady flowfield however, the physically small nature and large concentration of smoke particulate make it impossible to follow individual particles and obtain pathlines. A complex unsteady or turbulent flowfield will also tend to disperse smoke in such a manner so as to allow visualization of overall dynamics, i.e. wakes, vortices, and separated flows, but individual pathlines cannot be visualized (Mueller 1983). In order to obtain pathlines in an unsteady or separated flowfield, a much larger individual particle size and lower concentration is needed. A particle must be large enough to allow itself to be followed visually, but light enough to respond to gradients in the flowfield. This can be accomplished for subsonic flows through the use of helium filled soap bubbles. Whereas smoke provides particulate matter on the order of 1 μm to 5 μm (Merzkirch 1987), nearly neutrally buoyant helium bubbles can be generated on the order of 1 mm to 4.75 mm (Anonymous 1988).

The bubbles are large enough to be followed individually throughout the flowfield, but still provide a particle density close to that of air. The "neutral" density of the bubble supposedly allows it to respond to changes in the flowfield and trace streamlines. A commercially available helium bubble generation system for flow visualization purposes has been available since the mid 1970's. Mueller (1983) and Kerho (1992) document several instances of various flow visualization studies which used the neutrally buoyant bubble system which range from the flowfield of a close-coupled canard to the internal flow of an engine cylinder. Unfortunately, no study can be found which documents the accuracy of the neutrally buoyant concept for flow visualization.

The purpose of this study is to investigate the accuracy of helium bubbles used as flow tracers in an incompressible potential flowfield and the extent to which a currently available bubble generation system can provide quantitative flowfield data. The current investigation involved experimental and computational phases. An experimental investigation was first conducted where the trajectories of individual bubbles were acquired in the stagnation region of a NACA 0012 airfoil at 0° angle of attack using a commercially available bubble generation system. These experimental results are then compared to calculated potential flow streamlines of an equivalent flowfield to determine the extent to which the bubble generation system provided accurate flow tracers. In order to better understand the results of this comparison the equation of motion for an individual bubble was studied so as to ascertain the various physical quantities which determine an individual bubble's trajectory. A computational model of the equation was then employed to calculate individual helium bubble trajectories in a potential flowfield so as to better understand the forces acting on a bubble by the surrounding fluid. The model was also used to determine the sensitivity of a trajectory to various physical properties such as bubble density.

2
Experimental set-up and procedure

These experiments were conducted in the subsonic wind tunnel at the University of Illinois at Urbana-Champaign. The tunnel is an open return type with a 3 by 4 foot test section capable of operating from 0 to 165 mph at Reynolds numbers up to 1.5×10^6 per foot. Honeycomb and four turbulence screens located in the settling chamber provide a test section turbulence level as low as 0.05%.

In the 2-D experiment, individual bubbles moving in a 2-D laser sheet near the stagnation region of a NACA 0012 airfoil were video taped. The NACA 0012 model used for the experiment had a chord of 0.5334 meters and was mounted vertically in the test section. Helium bubbles were generated using a commercially available system. The bubbles are approximately 1 mm to 4.75 mm in diameter and are formed by injecting helium into a special soap film through a concentric tube arrangement (Hale et al. 1971). A dual generator system was used with the bubble producing "head" being contained within "vortex filters" supplied by the same vendor. Bubbles are created in the "head" and injected into the "vortex filter" which creates a vortical flowfield used to filter out non-neutrally buoyant bubbles. The heads and filter set-up were located in the tunnel settling chamber just aft of the anti-turbulence screens. The bubble generation system was set according to the calibration data received from the manufacturer. The bubbles were illuminated by a 4-watt ion-argon laser sheet approximately 2 mm thick projected perpendicular to the airfoil surface.

A KODAK Ektapro motion analysis system was used to video tape the individual bubbles moving in the laser sheet in the stagnation region of the airfoil. The system consisted of an Ektapro 1000 image processor and Ektapro intensified imager. The system was connected to a 386-type PC. The image processor was operated at 1000 frames per second with an imager gain of 73 and a gate time of 70 μs. A 200 mm lens provided a field of view of approximately 35 mm^2 with a pixel resolution of 0.60 mm. After storing the images on digital video tape, the image processor was controlled by the PC using a software package called Motion Pro. The Motion Pro software controlled the imager and allowed a frame by frame analysis by which individual bubbles could be tracked. A schematic of the test set up is shown in Fig. 1.

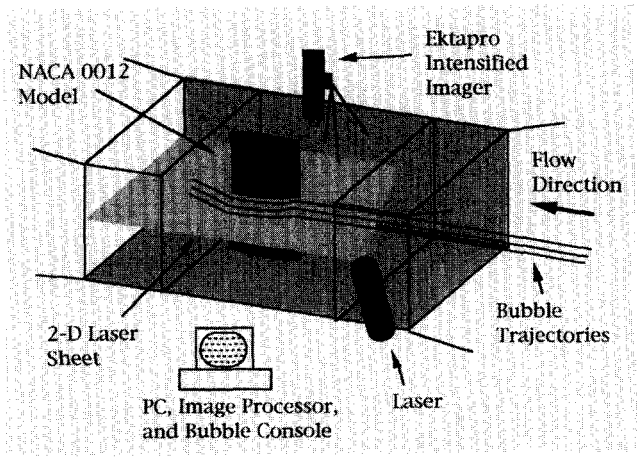

Fig. 1. 2-D experimental test section set-up schematic

The intensified imager was placed on the top of the test section looking down and leveled so as to provide a picture in the same plane as the 2-D laser sheet. Only bubbles within the sheet were illuminated and recorded by the imager, thereby insuring 2-D motion in the plane of the sheet. The accuracy of measurements made in this experiment relied heavily upon the proper alignment of the various instruments and airfoil. The laser sheet and imager must be in the same plane, and the plane of the laser sheet must be perpendicular to the leading edge of the airfoil. Markings on the airfoil at the stagnation point and 5% chord locations were illuminated by the laser sheet and provided a reference length for the velocity and coordinate calculations. Since the velocity and position measurements are made by determining a linear scaling factor from a reference length in the field of view, a misalignment of the imager or laser sheet would affect the scaling factor. For the pixel resolution of 0.60 mm, error bars for positional data in nondimensional form are ± 0.0022 $(x, y)/c$. The corresponding error bars for velocity data nondimensionalized by the freestream are ± 0.065. A free-stream velocity of 18 m/s (Re = 640,000) was chosen as it provided an acceptable number of data frames for a bubble passing through the field of view.

Due to the nature of the high speed digital system, a single digital video tape allowed for approximately 30 seconds of taping. During this time period three to four bubbles would enter the 2-D laser sheet in the stagnation region and be recorded. Trajectory data obtained were then further reduced and normalized by free-stream conditions. Velocity data were determined using a finite difference approach knowing the bubble position and the time between frames.

3
Results and discussion

Approximately fifty individual bubbles were tracked using the Ektapro video system. A comparison of several typical bubble trajectories to flowfield streamlines is given in Fig. 2. The flowfield streamlines were calculated using the Theodorsen

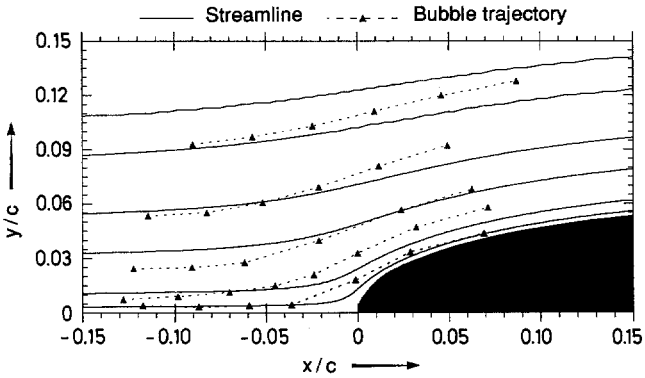

Fig. 2. Experimental bubble trajectories versus flowfield streamlines

method. From Fig. 2, the bubble trajectories are shown to deviate somewhat from the flowfield streamlines. The general trend of the helium bubbles was to cross over the streamlines, moving away from the airfoil. No bubble trajectories were observed to cross and track inside of the streamlines, moving towards the airfoil.

Since the helium bubbles were not tracing streamlines, a theoretical and computational study was performed so as to ascertain why the helium bubbles were not accurately following the flowfield streamlines. First the equation of motion for an individual particle was studied. A computational model of the equation was then employed.

Theoretical Analysis: Particles injected into a flowfield move relative to the surrounding fluid and have a finite response time to changes in that flowfield. The extent of this relative motion determines the accuracy of the particle as a flow tracer. The general equation of motion for a single rigid sphere is given by Maxey and Riley (1983):

$$m_p \frac{d^2 x_p}{dt^2} = \text{Drag} + \text{Bouyancy} + \text{Pressure} + \text{Apparent Mass Force} + \text{Basset Force} \quad (1)$$

For an incompressible, potential flowfield the individual force terms on the right hand side take the form:

$$\text{Drag} = \frac{1}{2}\rho C_D S |v_f - v_p|(v_f - v_p)$$

$$\text{Bouyancy} = (m_p - m_f) g_v$$

$$\text{Pressure} = m_f \frac{Dv_f}{Dt}$$

$$\text{Apparent Mass Force} = -\frac{1}{2} m_f \left(\frac{dv_p}{dt} - \frac{Dv_f}{Dt}\right)$$

$$\text{Basset Force} = 9 m_p \sqrt{\frac{\mu\rho}{\pi D^2 \sigma^2}} \int_0^t \frac{\frac{dv_f}{dt'} - \frac{dv_p}{dt'}}{\sqrt{t-t'}} dt' \quad (2)$$

For convenience and the purpose of this discussion, the left hand side of Eq. (1) can be defined as an inertial force. The Stokes drag term of Maxey and Riley used in (2) is replaced with a more general sphere drag coefficient expression. It is not clear at this point whether the helium filled soap bubble acts more like a water droplet in air or an air bubble in water. The effect of the drag for both cases was investigated and will be discussed later. Since the flowfield under study is incompressible and irrotational, the $\nabla^2 u$ term from Maxey and Riley's formulation has been dropped. Also, the apparent mass term has been modified to include the substantial derivative $\frac{Dv_f}{Dt}$, as per Auton (Maxey et al. 1983). An integral term, the Basset force decays with time as $t^{-1/2}$. Although included, the effect of the Basset force on the bubble trajectory for the flowfield and bubble size under study is very small and can be neglected.

Several assumptions are made in using this equation. Assumptions include that the physical size of a bubble and the concentration of the particles in the fluid are small enough that the bubbles have no effect upon each other or the surrounding flowfield. The bubbles are also assumed to remain spherical throughout their trajectory; an assumption that may be violated as the bubble experiences large transverse pressures and accelerations. This assumption will be addressed shortly. After nondimensionalizing the individual terms given in (2) by the free-stream conditions and model chord, the important nondimensional parameters which result include the inertia parameter K, a nondimensional particle mass given by $K = \sigma D^2 U_\infty / 18 c\mu$, the density ratio between the particle and the fluid, and the particle Reynolds number given by $Re_p = (\rho D U_\infty / \mu)|v_p - v_f|$.

The assumption that the bubble remains spherical in shape is a cause of possible error if the bubble is not neutrally buoyant. Error of this type would present itself if the shape of a non-neutrally buoyant bubble deviates from that of a sphere under large pressure gradients and accelerations. If a bubble deforms, the drag and pressure terms calculated by the trajectory equation will be in error. For the flowfield of this experiment the slip Reynolds numbers experienced along a trajectory by a near-neutrally buoyant bubble are small (<200) and the spherical assumption is justified. Very little has been done to study the distortion a bubble in air experiences as a result of acceleration or velocity. Work has primarily concentrated on drops in air or bubbles in liquids (Clift et al. 1978).

For a known flowfield, Eq. (2) can be used to calculate the trajectory of a helium bubble for various diameters and density ratios, i.e. neutrally buoyant and near-neutrally buoyant. A small particle following a flowfield streamline is primarily acted upon by pressure, inertial, and gravity forces. This particle can be thought of as a spherical volume having the same density as the fluid medium. The forces imposed upon the volume will cause it to perfectly trace the streamlines of a steady flowfield, or the pathlines of an unsteady flowfield. For a neutrally buoyant particle, the pressure forces balance the inertial forces present in Eq. (2) and the drag, Basset, and buoyancy forces are negligible and do not affect the trajectory. As long as the change in the flowfield properties are small over the diameter of the particle, a neutrally buoyant particle will follow the flowfield. For a non-neutrally buoyant particle the inertia parameter K becomes an important consideration. A particle having a small K value is intensely dominated by the drag term in (2) and can still faithfully follow the flowfield. For a particle with a large K value, however, the density ratio becomes important. For a near neutrally buoyant particle the drag is still small compared to the inertia-pressure balance. As a result, the fidelity to which

a large K value particle follows flowfield streamlines is more dependent upon its density ratio than its inertia parameter K. For the bubble in this study, K is of O(1). Referring to the dimensional terms described in (2), note that all terms on the right hand side except the pressure and buoyancy term are dependent either on slip velocities or slip accelerations. The gravity term is balanced by buoyancy forces in the flowfield. Therefore, in order to trace streamlines or pathlines, the slip velocities and accelerations present in the apparent mass, Basset, and viscous terms must be zero.

3.1
Computational model

A computational scheme developed by Bragg (1982) to calculate water droplet impingement trajectories has been modified to include the extra terms present in Eq. (2). This scheme uses the Theordorsen method to calculate the potential flowfield about an airfoil to obtain the pressures and velocities needed to solve (2). The use of this computational program allows a much better understanding of the physics involved as a bubble experiences flowfield gradients and provides a means of comparison to experimentally obtained trajectories. Figure 3 shows several neutrally buoyant bubble trajectories versus flowfield streamlines for a NACA 0012 airfoil section. From Fig. 3, the neutrally buoyant bubbles track the streamlines as expected. Even in the stagnation region a neutrally buoyant particle will negotiate the considerable flowfield gradients and trace streamlines. The drag coefficient for these calculations was that of Langmuir and Blodgett (Clift et al. 1978).

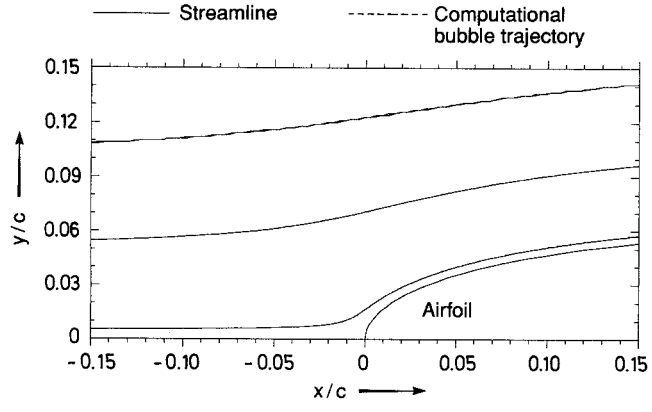

Fig. 3. Comparison of computational bubble trajectories to potential streamlines for a NACA 0012, $\alpha = 0°$

The effect of the density ratio upon an individual bubble trajectory can be determined by computing several trajectories while holding a constant diameter but varying the density ratio. The density ratio of a bubble is defined as the ratio of the bubble's density to the free-stream fluid density. Therefore, density ratios less than one denote a bubble which would rise in a stagnant flow, where those greater than one would fall. Bubbles with density ratios less than one will be termed "buoyant," those with ratios greater than one, "heavy." The effect of density ratio upon a given trajectory is depicted in Fig. 4. An isocontour of the pressure coefficient calculated from the Theodorsen code is also shown underlying the computational trajectories in Fig. 4. The pressure contour is useful as it provides insight into pressure forces experienced by the bubble.

From Fig. 4, the "buoyant" bubble with a density ratio of 0.80 tracks outside the neutrally buoyant trajectory and away from the airfoil. The "heavy" bubble, however, with a density ratio of 1.33 tracks inside the neutrally buoyant trajectory as its inertia carries it in towards the airfoil. For both non-neutrally buoyant bubbles, the balance between the pressure and inertial forces in the trajectory equation has been lost. As a result, neither the "heavy" nor "buoyant"bubble follow a streamline. Examining the pressure isocontour, as the bubble approaches the stagnation region, it experiences an increasing pressure. If inertial forces are not large enough to provide a balance to the pressure forces, the bubble is drawn away from the airfoil. If, on the other hand, the inertial terms outweigh the pressure, the bubble will move towards the airfoil.

An estimate of the error associated with a non-neutrally buoyant trajectory can be obtained by computing several trajectories with different density ratios and comparing these trajectories to flowfield streamlines. In estimating the error, however, it is important to note that the error associated with a given trajectory is highly dependent upon not only the local pressure gradient, but also upon the particle's trajectory up to that point. Two particles, for example, having different

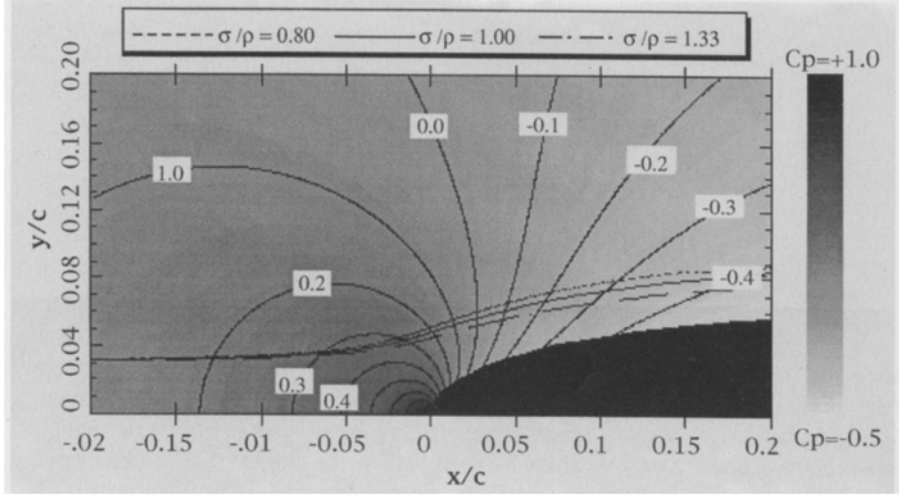

Fig. 4. The effect of density ratio on a computational bubble trajectory for a diameter of 3.0 mm

density ratios but the same diameter may pass through the same point in space yet have entirely different trajectories. As a result, one must be aware of the overall trajectory dynamics in order to define a meaningful error parameter. For the airfoil flowfield a relative error at a given spatial location can be determined. A normalized deviation for a trajectory at a given x/c location can be defined as:

$$\text{normalized deviation} = \frac{y_b - y_s}{h} \tag{3}$$

The normalized deviation is defined as the difference between the y/c location of the bubble trajectory (y_b) and the y/c of streamline (y_s) at a given x/c. The bubble trajectory and streamline originally coincide at the farfield boundary. This quantity is normalized by h, the difference of the streamline y/c at the farfield and the streamline y/c and the x/c location where the comparison is being made. For this normalization, a particle with infinite mass would impact the model on a straight trajectory giving a normalized deviation of -1; whereas a buoyant bubble's normalized deviation should approach a positive finite value as the density ratio is decreased ($+\infty$ if there were no drag). This normalization allows trajectories which begin at different y/c's to be compared at a given x/c location. Since for a given x/c, increasing y/c's provide less severe pressure gradients, the comparison allows the effect of density ratio and pressure gradient to be examined.

Figure 5 shows a plot of density ratio versus the normalized deviation from a streamline at the leading edge, $x/c = 0.00$, for three different y/c's, 0.02, 0.04, and 0.08. The dimensionless maximum pressure gradient along the originally tangent streamline for these y/c's are 6.47, 3.29, and 1.49 respectively.

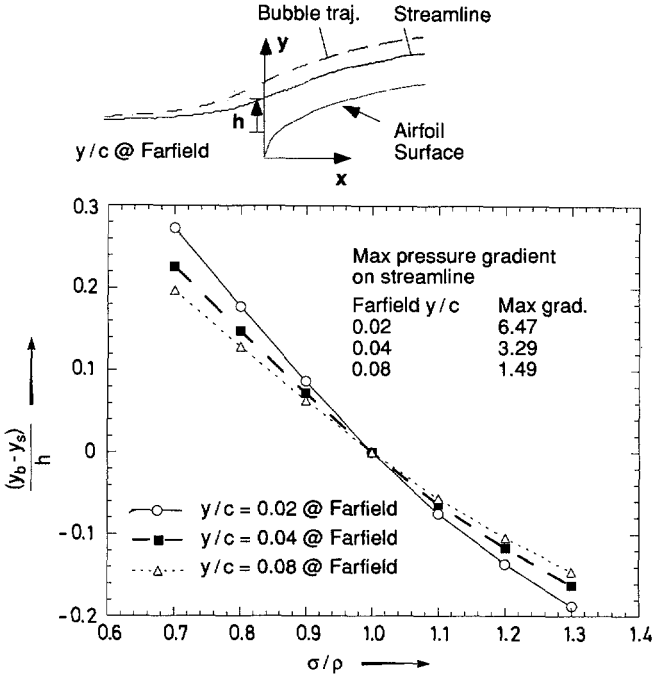

Fig. 5. Comparison of the normalized deviation versus density ratio for three different streamline y/c's in the farfield at $x/c = 0.00$ for a 3.00 mm diameter bubble

From Fig. 5, for a given y/c the normalized deviation is zero for a density ratio of 1, and increases as the ratio departs from 1. The range of density ratios is from 0.70 to 1.3 and covers the range of reasonably expected values. As the pressure gradient becomes less severe, the trajectory deviation from the streamline decreases as depicted by the lower normalized deviation of the larger y/c's. For example a bubble with a density ratio of 1.2, 20% from neutral, gives a normalized deviation of -0.136 for the most severe pressure gradient, -0.104 for the least severe gradient. On the other hand, a buoyant bubble with a density ratio of 0.80, still 20% from neutral, yields a normalized deviation of 0.177 for the most severe gradient, and 0.128 for the least severe. For a given pressure gradient a buoyant bubble will produce a larger normalized deviation than a heavy bubble with the same σ/ρ percentage deviation. The effect of changing the drag coefficient to that of a bubble in a liquid was also explored using the normalized deviation. The drag coefficient used for these calculations was a slightly modified form of Haberman and Mortons's and Lamb's found in Clift (1978). Since the drag term for the nearly neutrally buoyant bubble is small compared to the inertial and pressure terms in the trajectory equation, changing the drag coefficient had only a small effect. As the density ratio begins to depart more significantly from one, however, the difference in the drag coefficients will have a more pronounced effect upon the trajectory.

The computational and theoretical analysis of the equation of motion for a bubble trajectory has verified the assumption that a neutrally buoyant bubble will trace flowfield streamlines for the flowfield of interest. Due to the bubble's large K values, however, in extreme gradients, such as shock waves or flowfield discontinuities, the frequency response of the bubble might be less than desirable. The sensitivity of the bubble trajectory to its density ratio and the flowfield pressure gradient has also been observed. These elements appear to be the dominant factors in determining a bubble's trajectory.

3.2
Review of experimental results

Using the results of the theoretical and computational study it was now possible to obtain a better understanding of the experimental results. Recalling the behavior of the buoyant bubble trajectories discussed in the computational section above, the experimentally acquired trajectories appear to be the result of buoyant density ratios. The experimental trajectories track outside the streamlines away from the airfoil as shown in Fig. 2. Since it was suspected that the experimental trajectories were the result of buoyant density ratios, the computational model was used in an attempt to estimate the experimental bubble density ratio to verify this fact. The determination of the density ratio for an individual bubble in the acquired experimental trajectory was unavailable due to the difficulty in making such a measurement in-situ with the trajectory measurement. For the same reason, the bubble diameter could not be measured. In order to make an accurate determination of the bubble diameter, it would have to be verified that the bubble was at least half contained within the laser sheet and the measurement obtained using a macro lens set-up different from the lens used for the trajectory analysis. Stereo high-speed digital equipment of the type needed for this was not available to us. While this inhibited the measurement of the bubble diameter, it

does not have an effect upon the trajectory measurement. As a result, due to the lack of information on the bubble diameter and small number of experimental points per trajectory, it was possible to match more than one computational trajectory to an experimental trajectory over the small field of view encompassed by the experimental data. Therefore when individual experimental trajectories were matched, the diameter of the bubble was varied from 1 mm to 5 mm, the expected range of diameters (Anonymous 1988), while changing the density in order to "match" the experimental trajectory. The trajectory was "matched" by plotting the experimental data versus the computational data on an enlarged scale and visually identifying the best diameter-density ratio combinations. Although the trajectories are virtually identical over the range bounded by the experimental data, they do begin to slightly diverge downstream. The best fit trajectory results were then averaged to provide an estimation of the density ratio and diameter for the experimental trajectory. Approximately twenty trajectories were matched. Only trajectories relatively close to the airfoil surface which experience the largest pressure gradients were matched. Figure 6 depicts a typical comparison of the computational and experimental trajectories.

From Fig. 6, the three different diameters and corresponding density ratios fit the experimental trajectory well. Estimated density ratios for the bubble ranged from 0.714 to 0.833. It was observed that as the diameter of the bubble decreased, a smaller density ratio was required to match the trajectory. As the diameter of the bubble is decreased, the magnitude of the pressure and inertial terms in Eq. (2) drop by the radius cubed, whereas the drag term is only decreasing by the radius squared. As a result, a more buoyant bubble is required to compensate for the increased drag. An isocontour of the pressure coefficient calculated from the Theodorsen code is also shown underlying the trajectory in Fig. 6. Examining the pressure isocontour in the same manner as was done in the computational section, as the bubble approaches the stagnation point, it experiences an increasing pressure. If inertial forces are not large enough to provide a balance to the pressure forces, the bubble is drawn outwards, away from the airfoil. The density ratio and diameter values depicted in Fig. 6 are typical for all the computational trajectories matched to the measured trajectories. All of the matched trajectories had a density ratio less than one.

In order to determine if the methods used in estimating the density ratios and diameters were reasonable, a calculation of the bubble wall thickness was performed. For a given density ratio and diameter, a bubble wall thickness can be calculated. Soap bubble wall thicknesses can vary from 0.01 μm to 1.3 μm (Isenberg 1978). Knowing the bubble film density and assuming a surface tension, an equation relating density ratio to diameter and wall thickness can be derived from a simple mass balance. The surface tension of the bubble solution is needed to calculate the pressure and density of the helium inside the bubble. Only an order of magnitude estimate for the surface tension is required to produce an accurate calculation due to the relatively low pressure difference across the bubble wall. A surface tension close to that of water was chosen. Equating the total mass of the helium bubble to the sum of the mass of its constituents:

$$\text{mass of bubble} = \text{mass of bubble solution} + \text{mass of helium}$$

$$\frac{4}{3}\pi r^3\sigma = \frac{4}{3}\pi(r^3-(r-\tau)^3)\rho_{\text{bfs}} + \frac{4}{3}\pi(r-\tau)^3\rho_{\text{helium}} \tag{4}$$

Rearranging and dividing through by the density of air, ρ:

$$\frac{\sigma}{\rho} = \frac{1}{\rho}\left[\left(1-\frac{\tau}{D/2}\right)^3(\rho_{\text{helium}}-\rho_{\text{bfs}})+\rho_{\text{bfs}}\right]$$

$$\rho_{\text{helium}} = \frac{P_\infty}{RT} + \frac{4\gamma}{(D/2)RT} \tag{5}$$

Figure 7 shows the estimated bubble diameters and density ratios plotted with wall thicknesses calculated using Eq. (5). From Fig. 7, the estimated values indicate an average bubble wall thickness of 0.2 μm to 0.3 μm. These values are well within the limits of measured bubble wall thicknesses quoted by Isenberg (1978). The grouping of the data around this average value indicates a relatively constant wall thickness.

Experimental bubble velocities were also compared to velocities at points along a streamline. For this comparison, a streamline was chosen that coincided with the initial position of a bubble trajectory. Velocities at points on the streamline are

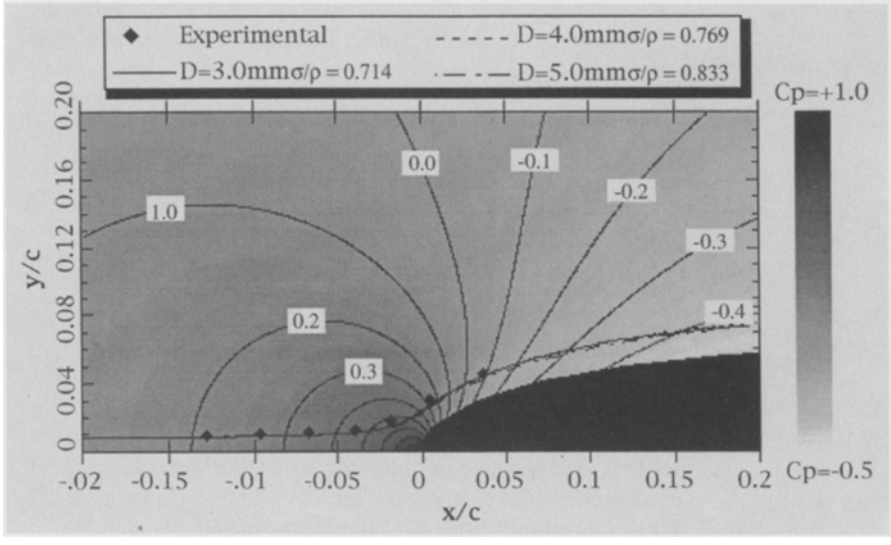

Fig. 6. Comparison of experimental and computational bubble trajectories for a typical buoyant bubble

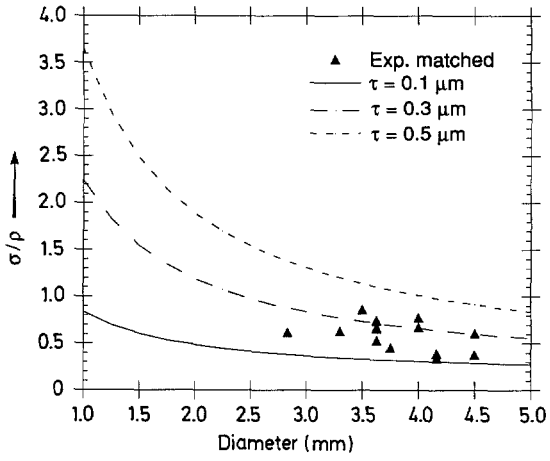

Fig. 7. Comparison of estimated diameter versus density ratio to wall thickness

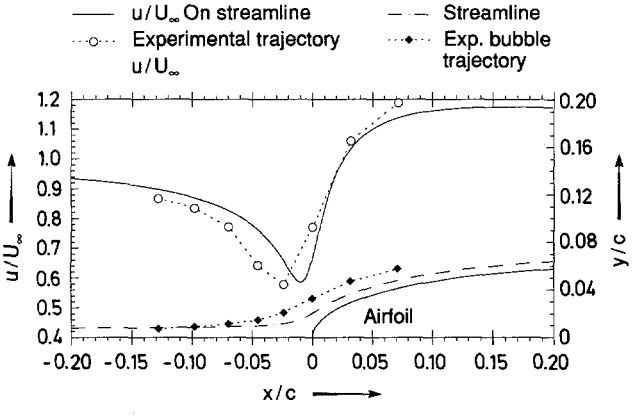

Fig. 8. Comparison of the streamwise component of velocity for an experimental bubble trajectory ($\sigma/\rho = 0.658$) to the streamwise velocity at points along a streamline

compared to the experimental bubble velocities at a given x/c. Figure 8 depicts a comparison of the streamwise component of velocity for a typical bubble versus the streamwise velocity on the streamline. The estimated density ratio for the bubble is $\sigma/\rho = 0.658$. The plot depicts velocity versus position on the left axis and the experimental trajectory and streamline on the right axis. From Fig. 8, examining the experimental trajectory and noting the estimated density ratio, the bubble is seen to be buoyant. Therefore, as the bubble approaches the stagnation region and experiences an increasing pressure force, its streamwise component of velocity is less at a given x/c than the velocity on the streamline. As the bubble begins to accelerate around the leading edge, its velocity increases beyond that of a point on the streamline.

A comparison of the normal or y component of velocity for the same bubble versus the streamline is shown in Fig. 9. The plot depicts velocity versus position on the left axis and the experimental trajectory and streamline on the right axis in the same format as used for Fig. 8. Again, since the bubble is buoyant and tracks outside the streamline, its normal velocity is greater at a given x/c than the corresponding point on the streamline for $x/c < 0$. At $x/c > 0$, the normal velocity appears to

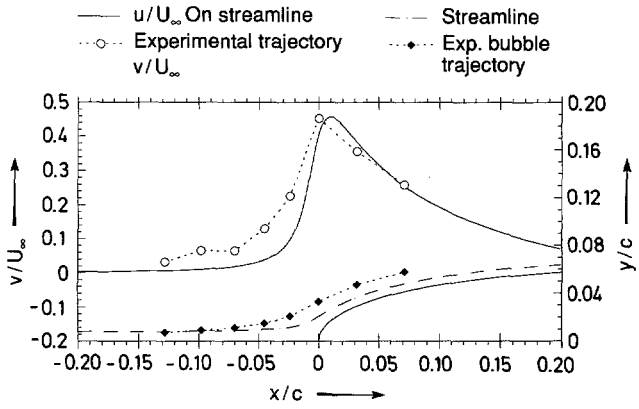

Fig. 9. Comparison of the normal component of velocity for an experimental bubble trajectory ($\sigma/\rho = 0.658$) to the normal velocity at points along a streamline

track with that of the streamline. By examining the trajectory position data, at $x/c > 0$ the bubble and streamline appear to follow parallel paths. The normal component of velocity should differ only if the trajectories are not parallel.

From the 2-D data obtained, the bubbles were generally shown to deviate somewhat from the streamlines. The effects of various density ratios upon the dynamics of the bubble motion indicate a strong relationship between flowfield pressure and inertial forces and bubble trajectories. Plots of the experimental trajectories and velocities agree well with trends observed in the computational study previously discussed. The experimental study revealed that all of the bubbles recorded were buoyant having density ratios less than one. None of the experimentally measured bubble trajectories had a density ratio greater than one. After an analysis of the bubble generation system itself, the range of "buoyant" density ratios and lack of "heavy" bubbles can be explained.

Focusing on the vortex filter, an examination of the physics involved revealed that the filter does not totally screen out non-neutrally buoyant bubbles and biases towards "buoyant" density ratios. The vortex filter operates by creating a vortex in a cylindrical tube with caps at both ends and a small hole in the center of one of the caps. Bubbles are injected tangentially at the wall into the filter. Only bubbles which are neutrally buoyant are reported to negotiate the vortex and spiral up and out the hole (Anonymous 1988). The general trends of the filter can be observed with a simple potential vortex. Keeping only the inertia and pressure terms, the equation of motion for a near-neutrally buoyant bubble will be reduced to Eq. (6) for simplicity:

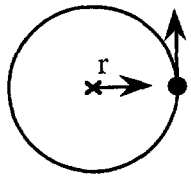

$$\frac{dv_p}{dt} = \frac{1}{\sigma} \nabla p \tag{6}$$

We know that for a potential vortex $v = \Gamma/(2\pi r)$, and it can easily be shown that through the use of Bernoulli's equation the pressure gradient across the bubble in the radial direction can be

written as:

$$\nabla p = \rho \left(\frac{\Gamma}{2\pi} \right)^2 \frac{1}{r^3} \tag{7}$$

Letting $\tilde{\Gamma} = \Gamma/(2\pi)$ for convenience, and using (7), the radial component of the equation of motion of the bubble can be written as:

$$\frac{dv_p}{dt} = \frac{1}{\sigma/\rho} \left(\frac{\tilde{\Gamma}^2}{r^3} \right) \tag{8}$$

For a mass of air moving around a potential vortex, the inertial force due to its centripetal acceleration balances the pressure force needed to maintain a perfectly circular path. The centripetal acceleration produced by the vortex is equal to:

$$a_c = \frac{v^2}{r} = \frac{\left(\frac{\Gamma}{2\pi r} \right)^2}{r} = \frac{\tilde{\Gamma}^2}{r^3} \tag{9}$$

Then rewriting Eq. (6) in terms of (8) and (9):

$$\frac{dv_p}{dt} = \frac{1}{\sigma/\rho} a_c \tag{10}$$

Therefore, from the relationship of (10) if $\sigma/\rho = 1$ then the particle acceleration equals the centripetal acceleration and the particle moves in a circle. If the particle is buoyant, with $\sigma/\rho < 1$, the particle acceleration is greater than the centripetal acceleration and the particle moves towards the center. By the same logic a heavy particle, $\sigma/\rho > 1$, moves towards the wall. Therefore, since the actual apparatus expels the bubbles through a hole in the center of the filter, those bubbles drawn to the center will be forced out of the filter. As a result, the filter screens out "heavy" bubbles and allows bubbles with density ratios of one or less, i.e. buoyant or neutrally buoyant bubbles to pass. The fact that no experimental bubbles with density ratios greater than one were recorded, adds strength to this argument.

Although the analysis has shown that the current bubble generation system produces a distribution of buoyant bubbles, the determination of the validity of data obtained through the use of the bubbles lies in the degree of accuracy required by the test. If only a global or qualitative measurement is required, or the pressure gradients are not large, then use of only neutrally buoyant bubbles is not imperative.

4 Conclusions

Research has been performed to determine the accuracy of helium bubbles and a commercially available helium bubble generation system for use as flow tracers in an incompressible potential flowfield. A two-dimensional experiment was conducted to experimentally determine bubble trajectories in the stagnation region of a NACA 0012 airfoil at 0° angle of attack. The equation of motion for a single bubble was obtained and evaluated using a computational scheme to determine the factors which affect a bubble's trajectory.

From the two-dimensional experiment, several trajectories were acquired in the stagnation region of the NACA 0012 at 0° angle of attack through the use of a high-speed digital video motion analysis system. The trajectories were shown to deviate somewhat from the flowfield streamlines. Since the bubbles were not tracing streamlines, they could not be neutrally buoyant. The computational scheme was used to estimate the physical properties of the experimental bubble trajectories. All estimated density ratios were less than one. An analysis of the bubble generation system itself provided an explanation for the large number of buoyant bubbles detected. The vortex filter was found to screen out only the heavy bubbles which have a density greater than that of air, and allow the buoyant as well as the neutrally buoyant bubbles to escape. The theoretical and computational results have shown, within the assumptions made in this analysis, that neutrally buoyant bubbles will trace flowfield streamlines. If a bubble is not neutrally buoyant, the amount of the deviation, or error, is greatly dependent upon the bubble's density ratio and the magnitude of the local pressure gradient. The two-dimensional experiment and analysis have shown that the use of the bubbles to trace flow patterns should be limited to qualitative measurements unless care is taken to ensure the production of neutrally buoyant bubbles by the generation system. If only a qualitative measurement is required, then the use of only neutrally buoyant bubbles is not imperative. The current system provides visualization of streamlines and pathlines in flowfields not easily visualized by traditional methods.

References

Anonymous (1988) SAI Bubble Generator: Description and Operating Instructions. Sage Action, Inc., New York, May 1988

Basset AB (1888) A Treatise on Hydrodynamics, Volume Two, Deighton, Bell, and Co., pp 285–297

Bragg MB (1982) Rime Ice Accretion and its Effect on Airfoil Performance. NASA CR 165599, March 1982

Clift R; Grace JR; Weber ME (1978) Bubbles, Drops, and Particles. Academic Press, New York

Hale RW; Tan P; Stowell RC; Ordway DE (1971) Development of an Integrated System For Flow Visualization In Air Using Neutrally Buoyant Bubbles. SAI-RR 7107, Dec. 1971

Isenberg C (1978) The Science of Soap Films and Soap Bubbles. Tieto Ltd., England

Kerho MF (1992) A Study Of The Accuracy Of Neutrally Buoyant Bubbles Used As Flow Tracers In Air. Masters Thesis, The University of Illinois at Urbana-Champaign, pp 24–26, 74–76

Maxey MR; Riley JJ (1983) Equation of motion for a small rigid sphere in a nonuniform flow. Physics of Fluids: 26 (4),

Merzkirch W (1987) Flow Visualization. Second Edition, Academic Press, Inc., New York, pp 1, 14–51

Mueller TJ (1983) Flow visualization by direct injection. In: Fluid Mechanics Measurements (ed. Goldstein, RJ). Hemisphere Publishing Corp., New York, pp 307–352